ARTICLES
PUBLISHED ONLINE: 21 NOVEMBER 2010 | DOI: 10.1038/NCHEM.901
nature chemistry

# Guest-induced growth of a surface-based supramolecular bilayer

Matthew O. Blunt[1], James C. Russell[1], Maria del Carmen Gimenez-Lopez[2], Nassiba Taleb[2], Xiang Lin[2], Martin Schröder[2], Neil R. Champness[2]* and Peter H. Beton[1]*

**Self-assembly of planar molecules on a surface can result in the formation of a wide variety of close-packed or porous structures. Two-dimensional porous arrays provide host sites for trapping guest species of suitable size. Here we show that a non-planar guest species ($C_{60}$) can play a more complex role by promoting the growth of a second layer of host molecules (*p*-terphenyl-3,5,3″,5″-tetracarboxylic acid) above and parallel to the surface so that self-assembly is extended into the third dimension. The addition of guest molecules and the formation of the second layer are co-dependent. Adding a planar guest (coronene) can displace the $C_{60}$ and cause reversion to a monolayer arrangement. The system provides an example of a reversible transformation between a planar and a non-planar supramolecular network, an important step towards the controlled self-assembly of functional, three-dimensional, surface-based supramolecular architectures.**

Two-dimensional molecular self-assembly at surfaces mediated by weak, non-covalent interactions leads to the formation of networks with a wide variety of different forms and potential functionalities[1–3]. Reports of several examples of close-packed[4,5] and porous[6–9] structures on surfaces have a particular focus on the construction of templates capable of trapping guest molecular species[7,10–15]. In several cases guest molecules were shown to play a more complex role than simple passive occupation of voids within a network; instead, they actively promote transformations of the host framework between different two-dimensional configurations[16–18]. We report here the use of a non-planar guest that, when trapped in a two-dimensional framework on a surface, promotes a new mode of supramolecular growth into the third dimension perpendicular to the surface. Despite the extensive interest in the field of supramolecular templates, there are no previous examples of the growth of such networks perpendicular to the surface. The guest species, chosen as the fullerene $C_{60}$ (**2**), has a near-spherical shape and simultaneously experiences stabilizing intermolecular interactions with molecules in both the first and second layer of a supramolecular bilayer. Furthermore, we find that the trapping of $C_{60}$ and growth of the second layer of the supramolecular framework are co-dependent, which confirms a cooperative addition of host and guest species. Significantly, the growth of the bilayer network may be reversed subsequently by the addition of coronene, a planar molecule that displaces the $C_{60}$ and destabilizes the bilayer structure, which leads to reversion to a monolayer arrangement. Overall, this system provides an example of a reversible transformation between a planar and a non-planar supramolecular network, an important step towards the controlled self-assembly of functional, three-dimensional, surface-based supramolecular architectures.

## Results and discussion

Guest-induced perpendicular growth of a surface-based hydrogen-bonded network is observed following the addition of $C_{60}$ (**2**) to an adsorbed monolayer of the molecule *p*-terphenyl-3,5,3″,5″-tetracarboxylic acid (TPTC, **1**). The molecular structure of TPTC, shown in Fig. 1a, consists of a terphenyl backbone linked to four carboxylic acids. These side groups promote intermolecular hydrogen bonding and two possible relative placements of neighbouring molecules are stabilized by these interactions, as shown in Fig. 1a[6,17,19]. When adsorbed at the solid–liquid interface between highly oriented pyrolytic graphite (HOPG) and nonanoic acid (**4**), TPTC forms an extended monolayer array of hexagonal pores separated by 16.6 Å and stabilized by in-plane hydrogen bonding. A schematic of the resulting supramolecular monolayer is shown in Fig. 1b and in this paper we focus on the potential of the hexagonal pores to act as host sites for guest molecules[7,10–15].

An interesting feature of the TPTC monolayer structure is that the pores are not all equivalent and we find a variation in the probability of trapping the guest molecules at different sites. The various hexagonal pores that combine to form the monolayer are shown in Fig. 1c (pores A–E). The pores are constructed from combinations of hydrogen-bonded dimers, as shown in Fig. 1a, and are composed of three (pore A), four (B, C), five (D) or six (E) molecules. The edges of these hexagonal units are formed either by the terphenyl backbone of TPTC (**1**) or by hydrogen-bonded junctions between carboxylic acid groups, which for this particular molecule have approximately equal lengths so that all the hexagonal pores (A–E) have, to a good approximation, equal dimensions. TPTC monolayers were investigated previously using scanning tunnelling microscopy (STM), and images similar to those published previously[6] are included in the Supplementary Information.

To investigate the possible capture of guest molecules, we first formed a TPTC monolayer on freshly cleaved HOPG (see Supplementary Information for full experimental details), and then added a small quantity of a saturated solution of $C_{60}$ in nonanoic acid (**4**). The STM image of the resultant HOPG–solution interface (Fig. 1d) shows the network structure obtained approximately 24 hours after the addition of the $C_{60}$ solution. The bright features in Fig. 1d correspond to individual $C_{60}$ molecules sited within pores with a minimum $C_{60}$–$C_{60}$ distance measured as ~16.5 Å, in good agreement with the measured pore–pore spacing of the TPTC network[6]. This suggests that $C_{60}$ adsorption occurred in some, but not all, of the pores in the TPTC network. In Fig. 1d ~53% of the pores are occupied by $C_{60}$.

[1]School of Physics and Astronomy, University of Nottingham, University Park, Nottingham NG7 2RD, UK, [2]School of Chemistry, University of Nottingham, University Park, Nottingham NG7 2RD, UK. *e-mail: peter.beton@nottingham.ac.uk; Neil.Champness@Nottingham.ac.uk

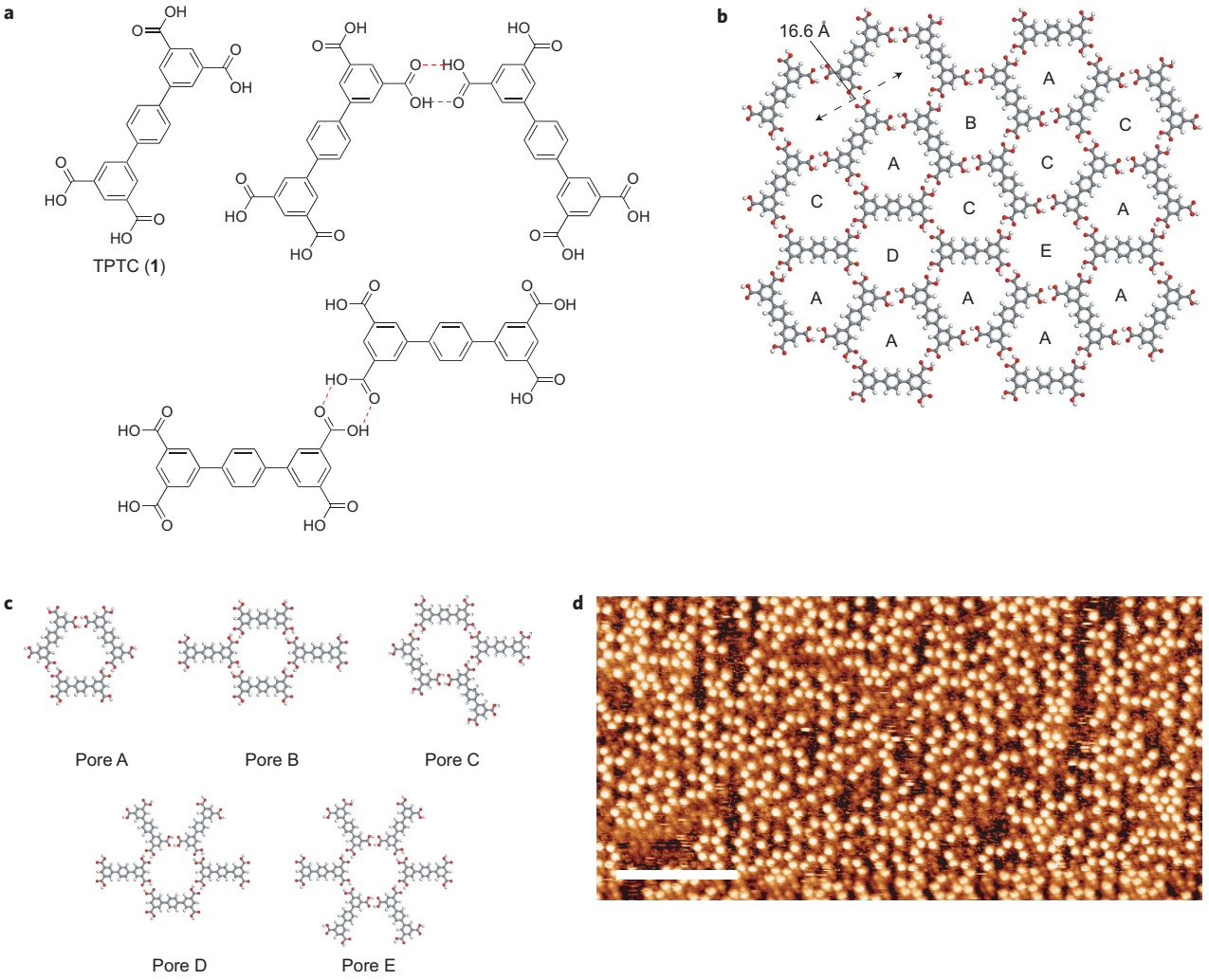


**Figure 1 | Molecular structure of TPTC single-layer network. a**, Molecular structure of TPTC and arrangements for hydrogen-bonded TPTC dimers with either the long axes of molecules mutually parallel or with one molecule rotated by 60°. **b**, Molecular schematic of a section of TPTC network that highlights the hexagonally ordered network of pores. The pore–pore separation (16.6 Å) is shown at the top left. **c**, Five possible arrangements of molecules that surround each pore within the TPTC network. The arrangements contain either three (pore A), four (pores B and C), five (pore D) or six (pore E) molecules. Examples of each of these pore types are labelled in (**b**). **d**, STM image of an area of TPTC network ~24 hours after deposition of $C_{60}$. The locations of $C_{60}$ are clearly visible as the bright spots in the image; the underlying TPTC network structure is not visible. Scale bar = 160 Å.

Although Fig. 1d shows the locations of the $C_{60}$ molecules it contains little information about the arrangement of the TPTC molecules that surround them. Using a defect in the HOPG substrate as a nucleation site, the growth of a small area of the $C_{60}$–TPTC network was tracked through sequential STM images. The STM images in Fig. 2 show a large, bright feature that corresponds to a HOPG surface defect. Growing outwards from this defect is an area of adsorbed $C_{60}$ molecules surrounded by a TPTC network. In the area where the $C_{60}$ molecules are adsorbed the TPTC molecules are visible as bright, rod-like features. As we show below this high contrast arises because these molecules are in the upper layer of a TPTC bilayer structure. In the areas that surround the adsorbed $C_{60}$ we observed a lower contrast layer, which corresponds to a TPTC monolayer adsorbed directly on graphite. The bilayer is fragile and regions can be removed by the STM tip, with subsequent regrowth (see Supplementary Information for examples).

A topographic cross-section through one of the STM scans is shown in Fig. 2b (the green line on Fig. 2c shows its location in the image). This cross-section confirms that a bilayer of TPTC was formed because the molecules in the monolayer have a significantly lower apparent height (~1 Å) than the TPTC molecules that directly surround the adsorbed $C_{60}$ (~2.5 Å). The peak height of a $C_{60}$ molecule is also shown on the cross-section (~6.5 Å) and is in good agreement with previously reported values for $C_{60}$, as recorded by STM[20]. These apparent heights include contributions from variations in the local density of states and, therefore, differ from simple estimates of molecular dimensions. The apparent heights observed in the STM images indicate that the TPTC (**1**) molecules in the region close to the adsorbed $C_{60}$ (**2**) form part of a second, overlying layer of TPTC network, which confirms the presence of a bilayer structure. We stress that neither $C_{60}$ adsorption nor second-layer TPTC growth is observed in isolation, which indicates a co-dependence of these processes. The role of the guest molecule and the co-dependence of $C_{60}$ inclusion and of TPTC bilayer formation distinguish the current study from previous examples of surface bilayer growth[21].

The adsorption sites in the TPTC monolayer that capture $C_{60}$ may be determined by monitoring the growth of the bilayer structure. The three STM images in Fig. 2d–f track the growth that originated from the HOPG substrate defect in Fig. 2a. Once incorporated into the $C_{60}$–TPTC bilayer the $C_{60}$ molecules, apart from a

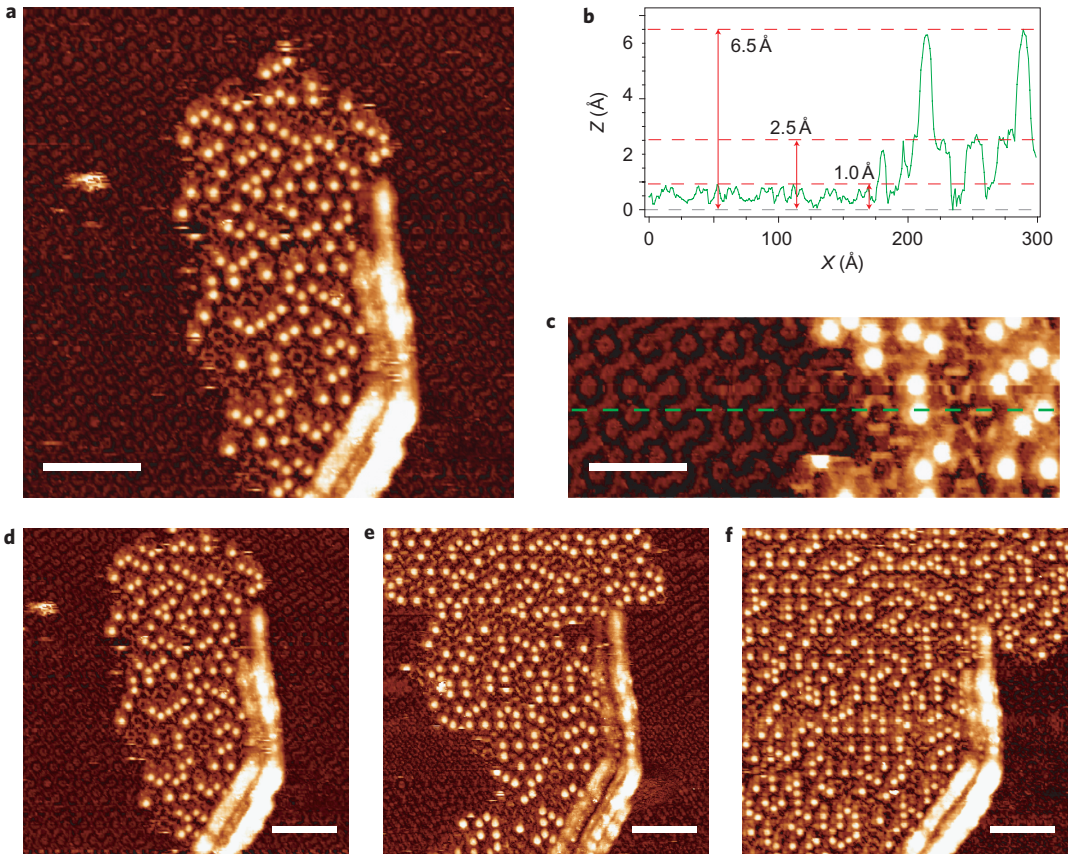


**Figure 2 | Growth of the TPTC–$C_{60}$ bilayer. a**, STM image of TPTC network immediately after $C_{60}$ deposition. An island of $C_{60}$ and bilayer TPTC network grows outwards from a surface defect. The initial layer of TPTC network is visible with an altered contrast (see Supplementary Information) and the TPTC molecules in the second layer appear with the long axis of the molecules as bright, rod-like features. Scale bar = 110 Å. **b**,**c**, Height profile (*Z*) taken through the edge (*X*) of the bilayer–$C_{60}$ island (**b**). The location of the height profile is marked with a green dashed line on the magnified STM image (**c**). Scale bar = 60 Å. **d–f**, STM images that show the growth of the bilayer–$C_{60}$ island; the time between images is approximately five minutes. All images were acquired with a tunnelling current of 20 pA and a tip bias of +1.2 V. Scale bars = 100 Å.

few exceptions, remained in fixed locations and can be used as reference points to map accurately the registry between the $C_{60}$ and the TPTC monolayer. The outer regions of the STM image shown in Fig. 2a were used to determine the configuration of TPTC molecules in the uncovered initial network layer. Using this approach we determined the molecular configuration of pores in the TPTC monolayer that later trap $C_{60}$ molecules in the final bilayer structure. The results from this analysis are summarized in Table 1, in which the first row shows the fractional occurrence of pore types (A–E, see Fig. 1c) for the TPTC monolayer regions and the second row shows the fraction of trapped $C_{60}$ in each pore type. The results show a strong preference for adsorption in pores of type A, which make up ~40% of pores in the initial layer but ~76% of pores that trap a $C_{60}$ molecule. All other pores show a lower-than-expected $C_{60}$ trapping occupancy (Table 1).

Also tabulated is the trapping energy for $C_{60}$ in each pore type of a TPTC monolayer calculated using molecular dynamics, using a previously reported method for carboxylic acids on HOPG (see Supplementary Information for details). There is a clear correlation between capture probability (ratio of pore occurrence to occupation fraction (Table 1)) and calculated binding energy, with the most stable configuration being a $C_{60}$ trapped in pore A (−2.20 eV) and the least stable a $C_{60}$ trapped in pore E (−1.98 eV). The variations in binding energy arise from the differences in the internal dimensions of the pores. Edges that consist of a TPTC backbone protrude slightly into the pore, which gives rise to increased van der Waals interactions. Type A pores have the largest number of terphenyl edges and thus the smallest internal size and highest binding energy.

Figure 3 shows the overall structure, in cross-section (Fig. 3a) and top view (Fig. 3b), of a fullerene captured in type A pores in layers 1 and 2. The spherical shape of the fullerene cage means that the footprint of $C_{60}$ on the graphite surface is smaller than its molecular diameter. Furthermore, the cross-sectional area of intersection between the fullerene and TPTC molecules is different in the planes of layer 1 and layer 2 molecules. Consequently, we would expect the $C_{60}$–TPTC interactions to have different strengths for the two layers. In fact, our calculations show that the fullerene is

**Table 1 | Pore configurations – details of TPTC monolayers that trap $C_{60}$ molecules.**

| | A | B | C | D | E |
|---|---|---|---|---|---|
| Fractional occurrence of TPTC monolayer pores (%) | 40 | 2.9 | 27 | 19 | 9.2 |
| Fraction of $C_{60}$ trapped in each pore type (%) | 76 | 1.6 | 15 | 6.2 | 1.1 |
| Ratio of $C_{60}$ trapped to fractional occurrence | 1.9 | 0.6 | 0.6 | 0.3 | 0.1 |
| Calculated trapping energy (eV) of $C_{60}$ guests in pores in a single-layer TPTC on HOPG | −2.20 | −2.10 | −2.11 | −2.05 | −1.98 |

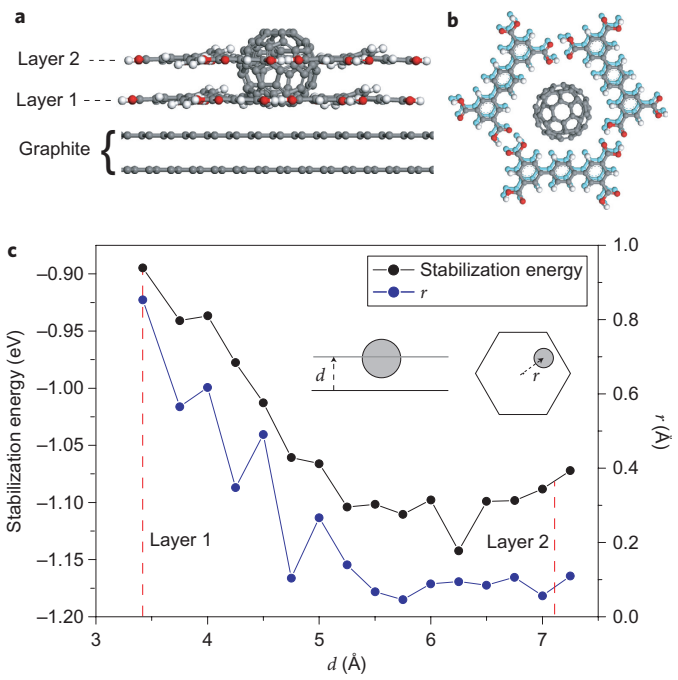


**Figure 3 | Structure of TPTC–$C_{60}$ bilayer. a**, Side-view of the $C_{60}$–bilayer network that consists of two overlying pores of type A. **b**, A top view of this arrangement with the $C_{60}$ placed at its minimum-energy position for both the first- (light blue) and second-layer pores (grey). The two layers are displaced slightly with respect to each other, which aids clarity, but in addition is expected on the basis of calculations (see text). **c**, Variation in stabilization energy and position for a $C_{60}$ in a single-layer pore of type A when the vertical position of the pore is varied from the equilibrium position for a first-layer pore (3.4 Å) up to just above that for an equilibrium position for a second-layer pore (7.25 Å). Red dashed lines show the equilibrium vertical positions for layers 1 and 2.

stabilized in a non-central position within a hexagonal TPTC monolayer pore and is offset by a displacement, $r$, towards a hydrogen-bond type of edge. The value of $r$ depends on $d$, the vertical offset between the graphite surface and the plane of the TPTC molecules (see inset to Fig. 3c).

In Fig. 3c the calculated values for $r$ and $E$ (the interaction energy between the TPTC pore and the fullerene (interactions with the graphite surface are not included in this value)) are plotted against $d$ for pore A. We find that for $d = 3.4$ Å, which corresponds to the height of a TPTC monolayer, the displacement $r$ is ~0.8 Å, whereas for a second-layer TPTC, for which $d = 7.1$ Å and $r \sim 0.1$ Å. Analogous results for pores B–E are included in the Supplementary Information and show that as the number of terphenyl edges is reduced the trapping energy is lowered and the displacement $r$ is increased. These results imply a relative lateral displacement of ~0.6 Å between layer 1 and layer 2 framework molecules if interactions are maximized in both layers simultaneously, although such a small offset cannot be determined directly from our images because of the resolution limitations.

It is also possible to use the growth sequence in Fig. 2 to analyse the positions of second-layer TPTC molecules relative to the first layer, and in particular to determine whether there is a preference for the adsorption of a terphenyl over another terphenyl or a hydrogen-bonded edge (this analysis does not include second-layer TPTC molecules directly adjacent to fullerene guests, for which STM tip convolution leads to limited resolution). Our results indicate that there is no preferred configuration and the distribution is consistent with random placement. Further details are provided in the Supplementary Information and our results show no evidence for a strong interaction between colocated oxygen atoms in the two layers. It is also interesting to consider why similar systems into which $C_{60}$ is introduced as a guest do not lead to bilayer or multilayer growth. In previous studies[10,19], $C_{60}$ was captured in a pore of type E and the analogous three-dimensional/bilayer growth would require a direct stacking of pores of this type. In the TPTC network studied here a bilayer can be formed without the

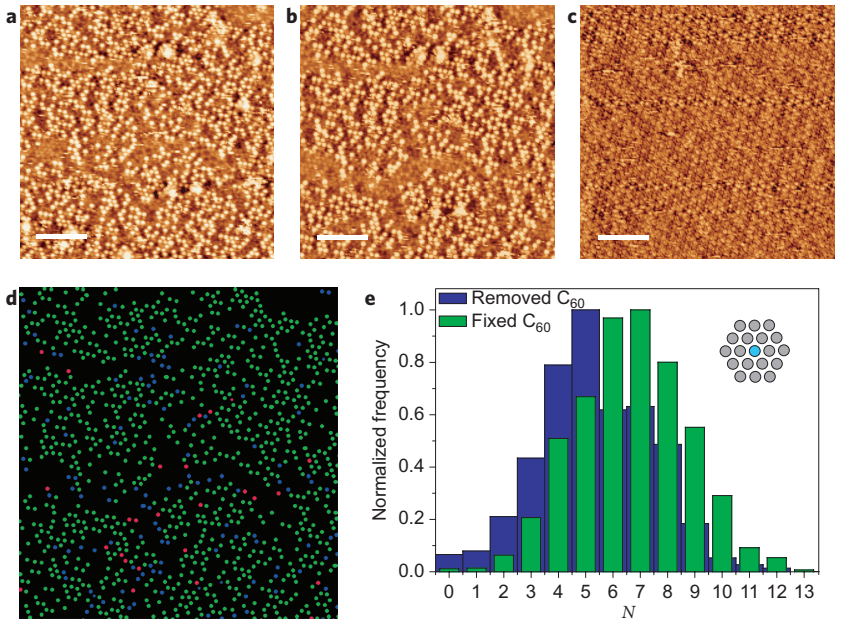


**Figure 4 | Reversal of bilayer formation by the addition of coronene. a–c**, Removal of the bilayer by coronene. Image (**a**) was taken approximately 20 minutes after the addition of the coronene solution, and images (**b**) and (**c**) after 40 and 60 minutes, respectively. Scale bars = 160 Å. **d**, Schematic view that shows the $C_{60}$ locations in (**a**) and (**b**). $C_{60}$ molecules that remain fixed in place between (**a**) and (**b**) are coloured green, removed $C_{60}$ molecules (those present in (**a**) but not in (**b**)) are coloured blue and recaptured $C_{60}$ molecules (those present in (**b**) but not in (**a**)) are coloured red. **e**, Histograms that detail the distribution of coordination number $N$ (number of occupied nearest-neighbour and next nearest-neighbour sites, see inset) for fixed $C_{60}$ (green) and removed $C_{60}$ (blue).

requirement to stack such pores – indeed, this structure is statistically unlikely because of the low occurrence and occupancy of type E pores. A possible explanation is that such stacking is energetically unfavourable and inhibits fullerene-mediated multilayer formation in trimesic acid and related supramolecular arrays[10,19].

The formation of the bilayer TPTC–$C_{60}$ network can be reversed by the addition of coronene (**3**) as a second guest molecule. Figure 4a–c shows STM images taken 20 (Fig. 4a), 40 (Fig. 4b) and 60 (Fig. 4c) minutes, respectively, after the addition of 10 μl of a solution of coronene in nonanoic acid (**4**) (0.0015 mg $ml^{-1}$) to the sample. After the addition of coronene, the bilayer–$C_{60}$ network was replaced by a single-layer TPTC network with coronene immobilized within its pores (coronene is trapped preferentially in pores of type E, as demonstrated previously by Griessl *et al.*[22]). Initially, this process proceeded relatively slowly with a reduction in the number of $C_{60}$ molecules of ~10% in 20 minutes (Fig. 4a and Fig. 4b). However, after 40 minutes (Fig. 4c) the $C_{60}$–bilayer structure was removed completely, which suggests a sudden onset of removal of $C_{60}$ and the absorption of coronene.

The removal of $C_{60}$ is non-random and displays spatial correlations, as shown in Fig. 4d in which the positions of fullerene molecules removed between the acquisitions shown in Fig. 4a,b are highlighted (removed molecules are blue, fixed molecules are green—a small number of newly trapped $C_{60}$ appeared and are marked red). This mapping shows that the initial fullerene adsorption is concentrated in small islands with lateral dimensions ~250 Å, around which there are boundaries where no fullerene adsorption occurs. This is consistent with islands of fullerene–TPTC nucleating at separate sites and growing into small, disconnected domains. The removal of $C_{60}$ guests (blue) is concentrated at the edge of these domains, as confirmed by a histogram (Fig. 4e) of the coordination numbers ($N$, the number of nearest-neighbour and next nearest-neighbour sites occupied by a $C_{60}$) that remain fixed (green) or are removed (blue). The histogram peak is at a lower value, $N = 5$, for the removed molecules than for the fixed molecules (peak at $N = 7$). This implies that the coronene-induced, second-layer removal occurred at domain edges in a reversal of a growth process. Interestingly, the occurrence of such domains indicates that a second-layer island nucleated in a TPTC monolayer does not continuously join an island nucleated at a different site. This suggests that second-layer islands nucleated at different sites can have variations in their registry with the first TPTC layer. This is consistent with the non-central adsorption site of the $C_{60}$ discussed above, which leads to at least six non-equivalent registries of the bilayer.

The demonstration that non-planar guest molecules may be used to promote the formation of supramolecular bilayers opens up a wide range of new possibilities for the formation of functional three-dimensional supramolecular architectures. The reversible nature of the growth process highlights the delicate balance of interactions required for perpendicular growth and provides an example of a responsive system in which guest exchange leads to changes in dimensionality.

Received 4 June 2010; accepted 7 October 2010;
published online 21 November 2010

## References

1. Bartels, L. Tailoring molecular layers at metal surfaces. *Nature Chem.* **2,** 87–95 (2010).
2. Elemans, J. A. A. W., Lei, S. B. & De Feyter, S. Molecular and supramolecular networks on surfaces: from two-dimensional crystal engineering to reactivity. *Angew. Chem. Int. Ed.* **48,** 7298–7332 (2009).
3. Barth, J., Costantini, G. & Kern, K. Engineering atomic and molecular nanostructures at surfaces. *Nature* **437,** 671–679 (2005).
4. Adisoejoso, J. *et al.* Two-dimensional crystal engineering: a four-component architecture at a liquid–solid interface. *Angew. Chem. Int. Ed.* **48,** 7353–7357 (2009).
5. Chen, W. *et al.* Two-dimensional pentacene: 3,4,9,10-perylenetetracarboxylic dianhydride supramolecular chiral networks on Ag(111). *J. Am. Chem. Soc.* **130,** 12285–12289 (2008).
6. Blunt, M. O. *et al.* Random tiling and topological defects in a two-dimensional molecular network. *Science* **322,** 1077–1081 (2008).
7. Theobald, J. A., Oxtoby, N. S., Phillips, M. A., Champness, N. R. & Beton, P. H. Controlling molecular deposition and layer structure with supramolecular surface assemblies. *Nature* **424,** 1029–1031 (2003).
8. Stepanow, S. *et al.* Surface-assisted assembly of 2D metal–organic networks that exhibit unusual threefold coordination symmetry. *Angew. Chem. Int. Ed.* **46,** 710–713 (2007).
9. Tahara, K. *et al.* Two-dimensional porous molecular networks of dehydrobenzo[12]annulene derivatives via alkyl chain interdigitation. *J. Am. Chem. Soc.* **128,** 16613–16625 (2006).
10. Griessl, S. J. H. *et al.* Room-temperature scanning tunneling microscopy manipulation of single $C_{60}$ molecules at the liquid–solid interface: playing nanosoccer. *J. Phys. Chem. B* **26,** 11556–11560 (2004).
11. Madueno, R., Raisanen, M. T., Silien, C. & Buck, M. Functionalising hydrogen-bonded surface networks with self-assembled monolayers. *Nature* **454,** 618–621 (2008).
12. Ivasenko, O. *et al.* Supramolecular assembly of heterocirculenes in 2D and 3D. *Chem. Commun.* 1192–1194 (2009).
13. Schull, G. *et al.* Selectivity of single-molecule dynamics in 2D molecular sieves. *Adv. Mater.* **18,** 2954–2957 (2006).
14. Wahl, M., Stohr, M., Spillmann, H., Jung, T. A. & Gade, L. H. Rotation–libration in a hierarchic supramolecular rotor–stator system: Arrhenius activation and retardation by local interaction. *Chem. Commun.* 1349–1351 (2007).
15. Stepanow, S. *et al.* Steering molecular organization and host–guest interactions using two-dimensional nanoporous coordination systems. *Nature Mater.* **3,** 229–233 (2004).
16. Wu, D., Deng, K., He, M., Zeng, Q. & Wang, C. Coadsorption-induced reconstruction of supramolecular assembly characteristics. *ChemPhysChem* **8,** 1519–1523 (2007).
17. Blunt, M. *et al.* Directing two-dimensional molecular crystallisation using guest templates. *Chem. Commun.* 2304–2306 (2008).
18. Li, M. *et al.* Site-selective fabrication of two-dimensional fullerene arrays by using a supramolecular template at the liquid–solid interface. *Angew. Chem. Int. Ed.* **120,** 6819–6823 (2008).
19. Zhou, H. *et al.* Frustrated 2D molecular crystallization. *J. Am. Chem. Soc.* **129,** 13774–13775 (2007).
20. Keeling, D. L., Humphry, M. J., Moriarty, P. & Beton, P. H. Attractive mode manipulation of covalently bound molecules. *Chem. Phys. Lett.* **366,** 300–304 (2002).
21. Samorì, P., Severin, N., Simpson, C. D., Müllen, K. & Rabe, J. P. Epitaxial composite layers of electron donors and acceptors from very large polycyclic aromatic hydrocarbons. *J. Am. Chem. Soc.* **124,** 9454–9457 (2002).
22. Griessl, S. J. H. *et al.* Incorporation and manipulation of coronene in an organic template structure. *Langmuir* **20,** 9403–9407 (2004).

## Acknowledgements

We thank the UK Engineering and Physical Sciences Research Council for financial support under grant EP/D048761/1. M.S. thanks the European Research Council for an Advanced Grant. N.R.C. acknowledges the receipt of a Royal Society Leverhulme Trust Senior Fellowship.

## Author contributions

M.O.B. and J.C.R. acquired the STM data, M.O.B. performed the MD simulations, M.C.G, X.L., M.S. and N.R.C. developed the synthetic route for the TPTC molecule, M.O.B. and P.H.B. analysed the data, M.O.B., N.R.C. and P.H.B. conceived and coordinated the experimental work and M.O.B., N.R.C. and P.H.B. co-wrote the paper.

## Additional information

The authors declare no competing financial interests. Supplementary information and chemical compound information accompany this paper at www.nature.com/naturechemistry. Reprints and permission information is available online at http://npg.nature.com/reprintsandpermissions/. Correspondence and requests for materials should be addressed to N.R.C. and P.H.B.